Available online at www.sciencedirect.com

ScienceDirect

journal homepage: www.elsevier.com/locate/he

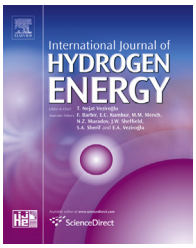

Theoretical investigations of the interaction between transition-metal and benzoquinone: Metal dispersion and hydrogen storage

Xiang Huang [a], *Yu-Jun Zhao* [a,b,c], *Ji-Hai Liao* [a], *Xiao-Bao Yang* [a,b,c,*]

[a] *Department of Physics, South China University of Technology, Guangzhou, 510640, People's Republic of China*
[b] *Key Laboratory of Clean Energy Materials of Guangdong Higher Education Institute, South China University of Technology, Guangzhou, 510640, People's Republic of China*
[c] *School of Materials Science and Engineering, South China University of Technology, Guangzhou, 510640, People's Republic of China*

ARTICLE INFO

Article history:
Received 23 February 2016
Received in revised form
5 May 2016
Accepted 5 May 2016
Available online 26 May 2016

Keywords:
Kubas-like interaction
H_2 storage
First-principle calculations

ABSTRACT

The dispersion of transition metals (TM) has been an ongoing challenge for quasi-molecular H_2 storage. Here we have investigated the adsorption of TM (Sc, Ti, V, Cr, Mn, Fe, Co, Ni, Cu, and Zn) on benzoquinone (BQ), by using the first-principles methods. It is found that Sc or Ti (Sc/Ti) atom is energetically favored to bind with ortho-BQ (OBQ) to form OBQ–Sc/Ti complex when compared to their bulk structures. Notably, the coordination number of Sc/Ti is only two, thereby providing enough empty *d* orbitals for H_2 storage without geometrical blocking. Four H_2 molecules can be accommodated by each OBQ–Sc complex via Kubas-like interaction, with the adsorption energy of 0.20 eV/H_2 and the H_2 storage capacity of ~5.0 wt%. For practical application, two types of structures have been proposed for H_2 storage using BQ molecule as building block, which would guarantee the dispersing of Sc atom and avoid clustering of OBQ–Sc complexes. In particular, for Sc-decorated oxygen-terminated zigzag graphene nanoribbons, the capacity of H_2 storage reaches up to 6.0 wt%.

Introduction

The Kubas-like interaction mechanism, derived from hybridization between *d*-orbitals of transition metal (TM) and H_2's σ/σ^* orbitals [1], is dominant for quasi-molecular H_2 storage based on TM-decorated nanomaterials [2–6]. A suitable binding energy of H_2 with TM (0.2–0.6 eV/H_2) endows these materials some outstanding properties, such as fast adsorption-desorption kinetics, good reversibility, and suitable desorption temperature [7–11], thus showing remarkable advantages towards nanostructure and metal hydride materials. To reach a higher H_2 storage, a better dispersion of TMs on adsorbent is required, which has been pointed out by the previous theoretical studies [12–14]. A typical illustration is Ti-decorated *cis*-polyacetylene [12,15,16], on which each isolated Ti atom could adsorb $5H_2$ molecules with binding energy as large as 0.46 eV/H_2. However, only $2H_2$ can be accommodated by a Ti clustered dimer via Kubas-like interaction with a weakened binding strength of 0.26 eV/H_2. Similar cases have

* *Corresponding author*. Department of Physics, South China University of Technology, Guangzhou, 510640, People's Republic of China.
E-mail address: scxbyang@scut.edu.cn (X.-B. Yang).
http://dx.doi.org/10.1016/j.ijhydene.2016.05.033
0360-3199/

been also reported for the system of Ti-decorated fullerene [3,13], where the clustering of Ti atoms does not only change the nature of H_2 bonding but also reduce the weight percentage of H_2 storage. Therefore, the search for novel supporting matrices that can disperse TMs has become the key issue for the design of H_2 storage media through Kubas-like interaction mechanism.

In the past decades, carbon-based nanostructures, BN nanostructures, organic polymers, and porous networks have been proposed as candidates to disperse TMs [2–4,14,17–21], considering their high surface-to-weight ratio and light weight. However, a serious obstacle is that the TM clustering is difficult to overcome, since the binding energy of TM with these materials is much smaller than its corresponding cohesive energy. A number of tactics for stabilization on surface have been attempted, such as doping via substituting C atom by B or N atom [6,22], introducing mono or double-vacancy [23], or their combinations [21,24]. In addition, using strain modulation [25] or curvature of nanostructure [26] has also been explored. However, a general confliction seems exist between the H_2 adsorption capacity and structural stability. A strong binding between TM and adsorbent is often accompanied with a large TM coordination number, and subsequently the number of adsorbable H_2 molecules and the binding strength via Kubas-like interaction are both significantly reduced [21,27]. For instance, through incorporating porphyrin unit as TM dispersants in graphene, TMs from Sc to Zn can be dispersed with each TM bonded with four N atoms, while each TM could adsorb no more than two H_2 molecules [21]. Thus, for an ideal H_2 storage media, the number of TM coordination should be small enough to enhance the H_2 adsorption, and meanwhile the binding between TM and adsorbent should be strong enough to maintain the system's stability.

In this paper, we have proposed an organic molecule benzoquinone (BQ) to disperse TM (TM = Sc, Ti, V, Cr, Mn, Fe, Co, Ni, Cu, and Zn) atoms. In the formed ortho-BQ–Sc or ortho-BQ–Ti (OBQ–Sc/Ti) complex, the binding energy is remarkably larger than Sc/Ti's cohesive energy and the coordination number of Sc/Ti is only two, indicating a well dispersion of TM and enough empty *d* orbitals for further H_2 uptake. Four H_2 molecules can be accommodated by each OBQ–Sc molecule via Kubas-like interaction, with adsorption energy of 0.20 eV/H_2 and H_2 storage capacity of 5.0 wt%. Using BQ molecule as building block, two types of structures have been designed for H_2 storage, the capacity of which are 3.8 and 6.0 wt%, respectively.

Computational methods

The spin-polarized calculations were carried out based on density functional theory (DFT) as implemented in Vienna *ab* initio simulation package (VASP) [28]. The exchange and correlation potential with the generalized gradient approximation of Perdew, Burke, and Ernzerh (GGA-PBE) [29] was combined with the projector-augmented wave method (PAW) [30] to solve the Kohn–Sham equations. Dispersion correction, which takes van der Waals interaction into account, is adopted at DFT-D2 level of Grimme method [31], which is known to give a better description of geometries and corresponding energies than those from the standard DFT [32].

The binding of TMs on OBQ and the H_2 molecules' adsorption on OBQ–Sc complex were simulated in a cubic box of 20 × 20 × 20 Å at Γ point with a cutoff energy of 480 eV. All the structures were relaxed until the force on each atom is less than 0.01 eV/Å. The optimized bond lengths of C_1–O, C_1–C_2, C_2–C_3 of para-BQ (PBQ) molecule are 1.24, 1.48, 1.35 Å, respectively, well consistent with the experimental data [33,34], and those of C_1–O, C_1–C_1, C_1–C_2, C_2–C_3, and C_3–C_3 of OBQ molecule are 1.23, 1.57, 1.47, 1.36, and 1.46 Å, in good agreement with previous theoretical studies [35] (cf. Fig. 1 and Table 1). The variation in total energy of configuration OBQ–Sc–4H_2 (cf. Fig. 2d) with the cell size increasing from 20 to 30 Å is within 3 meV. The binding energy of TM is defined as $E_b = (E_{OBQ} + nE_M - E_{OBQ-nM})/n$, where E_{OBQ}, E_M, and E_{OBQ-nM} represent the total energies of isolated OBQ molecule, isolated TM atom, and OBQ with adsorbed TMs respectively, and n is the number of TMs. The binding energies are listed in Table 2, combined with TMs' cohesive energies from theoretical calculations and experiments [36]. The Sc–O bond length in OBQ–Sc complex is 1.91 Å, close to ~2.07 Å in Sc_2O_3 compound [37]. The calculated cohesive energy of Sc is 4.14 eV, in agreement with the experimental value of 3.90 eV.

The O-terminated zigzag graphene nanoribbons (O-ZGRNs) is simulated by a periodical structure of $C_{16}O_8$ along the X-axis direction, the vacuum layers in Y and Z directions are both ~15 Å. The Brillouin zone is sampled using a Γ point centered *k*-mesh of 8 × 1 × 1. The lattice constant is 10.06 Å. In the optimized configuration (shown in the inset of Fig. 5), the bond lengths of C=O, C–C, and C=C are 1.23, 1.49, and 1.37 Å, consistent with the previous theoretical study [38].

Results and discussion

Transition metal dispersion and hydrogen adsorption

The BQ molecule ($C_6H_4O_2$) contains two isomers, i.e., 1, 4-BQ (PBQ) and 1, 2-BQ (OBQ). Structurally, they can be regarded as two H atoms of benzene (C_6H_6) at para or ortho -position replaced by two O atoms, as shown in Fig. 1a. The O atom is bonded with C atom via a C=O double bond. Consequently, the circular π-bond of benzene is broken. Instead, it appears as a planar structure with localized, alternating C=C (~1.36 Å), C–C (~1.47 Å), and C=O (~1.23 Å) bonds (c.f. Table 1). The OBQ is about 0.32 eV less stable than PBQ. It is likely ascribed to the electrostatic repulsion between two neighboring O atoms.

The BQ molecule exhibits a strong ability of capturing electron. When each carbonyl O atom obtains an extra electron, the double bond of C=O breaks and a *p* electron is released at the end of each carbonyl C atom. Together with four *p* electrons located at two C=C bonds, a circular π-bond forms on the ring plane, leading to an unsaturated carbon-ring transformed to a benzene. To illustrate this tendency quantitatively, we consider a reaction of H_2 dissociated to bond with two O atoms of OBQ to form 1, 2-benzenediol ($C_6H_6O_2$). The exothermic energy is 2.18 eV, in good agreement with the previous studies [39,40].

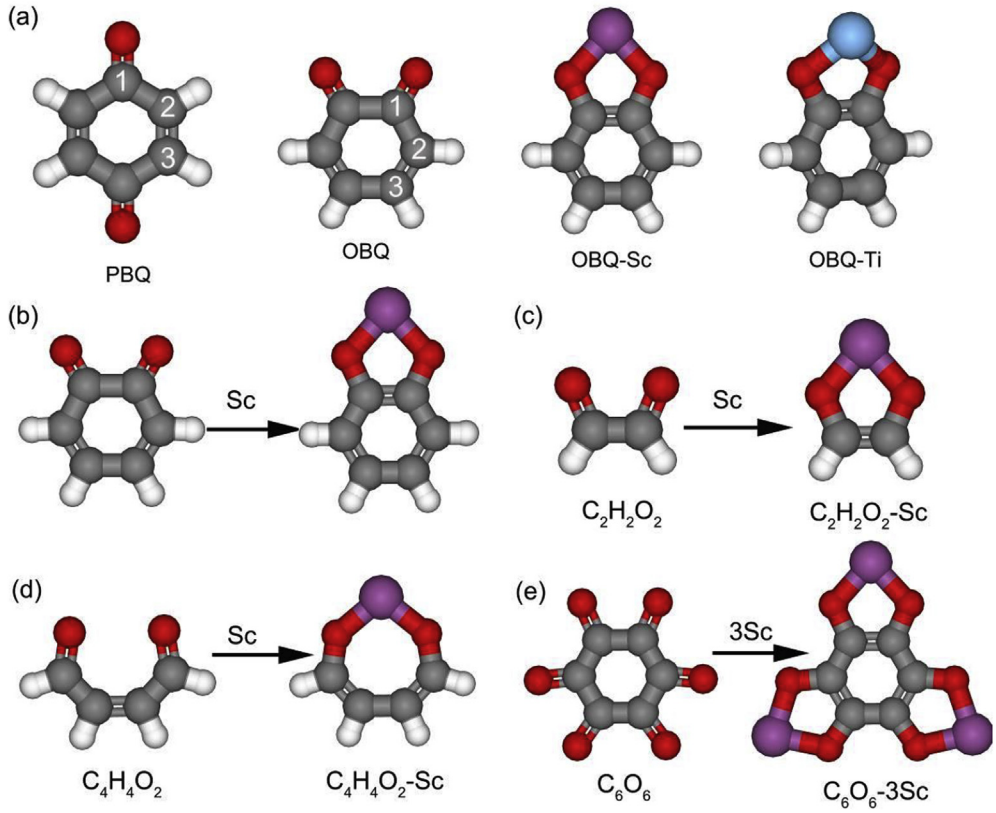

Fig. 1 – (a) Configurations of 1, 4-BQ (PBQ), 1, 2-BQ (OBQ), OBQ–Sc complex, and OBQ–Ti complex. (b)–(e) Schematic of reactions between Sc and OBQ, $C_2H_2O_2$ (hypothetical), $C_4H_4O_2$, and C_6O_6, respectively. The gray, red, white, purple, and light blue balls denote C, O, H, Sc, and Ti atoms, respectively. (For interpretation of the references to color in this figure legend, the reader is referred to the web version of this article.)

Adsorption of TM atoms on OBQ

Given this unique property, we investigate the adsorption of a single TM atom (TM = Sc, Ti, V, Cr, Mn, Fe, Co, Ni, Cu, and Zn) on an OBQ molecule to form OBQ–TM complex. Considering possible configurations, we find that TM is energetically favored to bond with two O atoms of OBQ, with no barrier for this adsorption process. The binding energies are listed in Table 2. Notably, the binding of Sc/Ti atom with OBQ shows greater stability compared to the Sc/Ti bulk structure. Especially, E_b of Sc is 2.24 eV larger than its cohesive energy, indicating a preferable dispersion by OBQ energetically.

Structurally, all the atoms of OBQ–Sc complex are in a plane. It is different from OBQ–Ti complex, where Ti atom slightly protrudes from the OBQ plane (c.f. Fig. 1). Nevertheless, the C–C bond lengths are close to 1.40 Å for both cases, except for a little deviation (~1%) for C_1–C_1 and C_1–C_2 bonds (resulted from the strain effect of formed five-member ring (C_2O_2–Sc/Ti)). In other words, the unsaturated carbon-ring of OBQ has converted to a benzene binding with Sc or Ti atom.

Table 1 – The bond lengths (c.f. Fig. 1 for the indexing of carbon atoms) of isolated PBQ and OBQ molecules, and complexes of OBQ–Sc and OBQ–Ti, respectively. The lengths of C–H bonds in all these configurations are 1.09 Å.

Configuration	TM-O	C_1–O	C_1–C_1	C_1–C_2	C_2–C_3	C_3–C_3
PBQ	–	1.24	–	1.48	1.35	–
OBQ	–	1.23	1.57	1.47	1.36	1.46
OBQ–Sc	1.91	1.37	1.42	1.39	1.40	1.40
OBQ–Ti	1.87	1.38	1.42	1.39	1.40	1.40

The total magnetic moment for OBQ–Sc/Ti complex is 1.0/2.0 μ_B, corresponding to two 4*s* electrons of Sc ($3d^14s^2$)/Ti ($3d^24s^2$) taken part in Sc/Ti–O bonding, in line with the above analysis. E_b for the second Sc/Ti atom binding with OBQ–Sc/Ti complex is 1.95/3.01 eV, significantly smaller than that of the first Sc/Ti atom and the cohesive energy of Sc/Ti bulk, showing straightforwardly that the clustering of Sc/Ti atoms on OBQ is not likely to happen once OBQ–Sc/Ti complex is formed. This is because each OBQ is capable to accommodate up to two electrons. Meanwhile, the electron deployment raises the electrostatic repulsion between two Sc/Ti atoms. Hence, the stable configuration is each OBQ molecule bonded with one Sc/Ti atom, i.e., OBQ–Sc/Ti.

Considering a remarkable dispersing ability of OBQ towards Sc/Ti atoms, we take OBQ–Sc complex as an instance to analyze the mechanism. From the structural change before and after adsorption (c.f. Fig. 1b), the binding energy can be ascribed to three parts of contributions: (i) Energy difference between formation of two Sc–O bonds and breakage of two C–O bonds; (ii) Formation of a C–C π-bond; (iii) Resonance energy resulted from the formation of a delocalized π-bond of the carbon-ring. To obtain the relative weight of each part quantitatively, we take a hypothetic

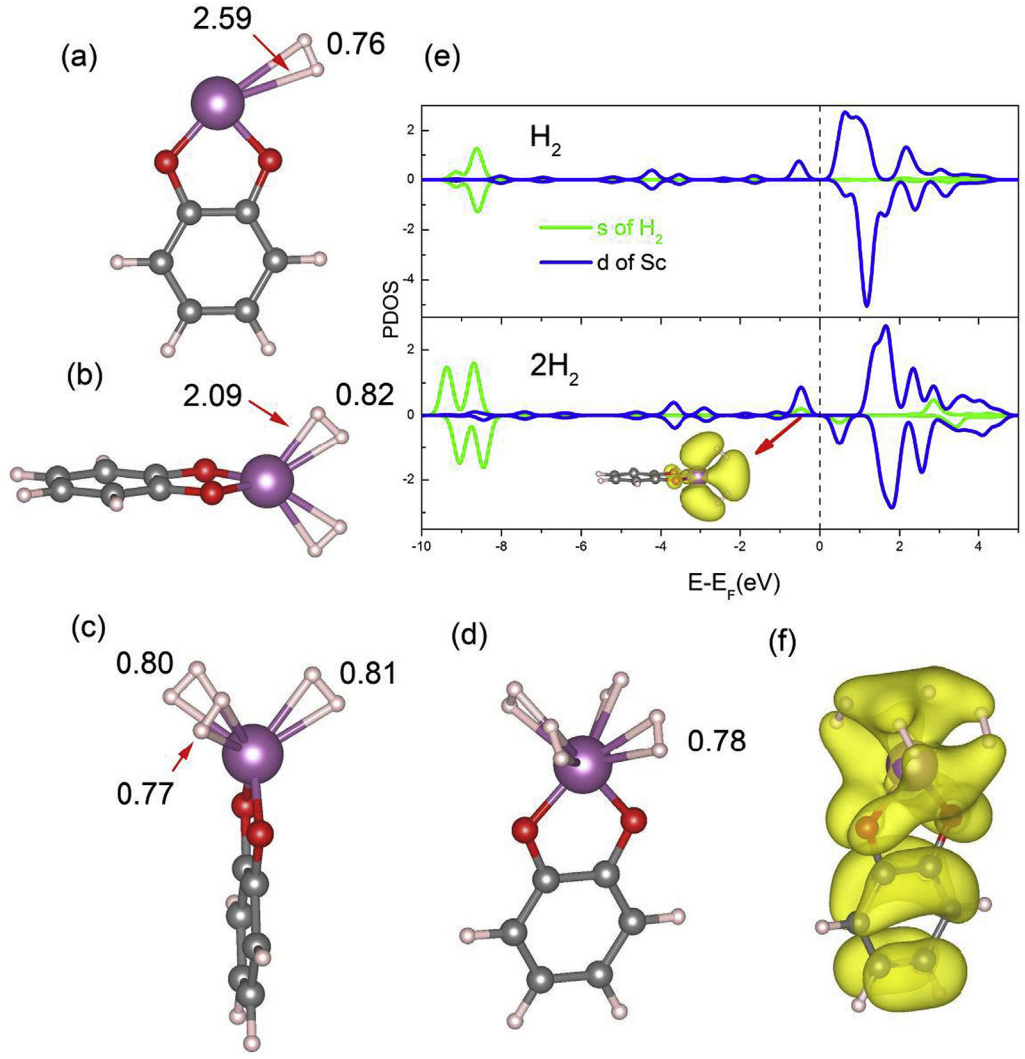

Fig. 2 – (a)–(d) Optimized configurations of four H_2 molecules adsorbed successively on OBQ–Sc complex. (e) PDOS of Sc and H_2 for the optimized configurations of OBQ–Sc–H_2 and OBQ–Sc–$2H_2$. The inset shows the partial charge density (PCD) of OBQ–Sc–$2H_2$. (f) PCD of OBQ–Sc–$4H_2$. Both of these PCDs are calculated in the energy range of [−1, 0] eV relative to Fermi level, with isosurface level 0.002 *e*/bohr^3. Note that obvious hybridization between σ* orbitals of H_2 and *d* orbitals of Sc, indicating Kubas-like interaction for Sc–H_2 bonding. The bond lengths are in Å.

Table 2 – Binding energies (E_b) of TMs (TM = Sc, Ti, V, Cr, Mn, Fe, Co, Ni, Cu, and Zn) interacting with OBQ, as well as the corresponding cohesive energies from calculations (E_{coh}^{cal}) and experiments (E_{coh}^{exp}) [36].

Element	Sc	Ti	V	Cr	Mn	Fe	Co	Ni	Cu	Zn
E_b(eV)	6.38	6.05	5.06	3.64	3.51	3.76	3.62	3.73	2.45	0.96
E_{coh}^{cal}(eV)	4.14	5.42	5.41	4.03	3.71	4.99	5.12	4.81	3.50	1.11
E_{coh}^{exp}(eV)	3.90	4.85	5.31	4.10	2.92	4.28	4.39	4.44	3.49	1.35

reaction between Sc atom and $C_2H_2O_2$ molecule of a fictitious structure for reference, in which only parts i and ii are included (c.f. Fig. 1c). The bond energy of π-bond, i.e., part-ii contribution, is estimated from C_2H_4 molecule. Roughly, the contribution is in the order of ii (2.80 eV) > i (2.55 eV) > iii (1.03 eV) (c.f. Table S1 in the supplemental material). Here, it should be stressed that the contributions of these three parts are only rough evaluations, which is beneficial for the understanding of interaction between OBQ and TM.

To one's surprise, it is found that the sum of parts i and ii is already greater than the cohesive energy of Sc. It implies that the molecules, as long as containing two adjacent C=O groups, are able to disperse Sc atoms. Here we searched two small molecules provided with this character, i.e., (Z)-2-butenedial ($C_4H_4O_2$) and C_6O_6. In the former case, two adjacent C=O groups are separated by a C=C bond. When bonded with a Sc atom, the C=C bond is broken and two new C=C bonds are formed, seen in Fig. 1d. The binding energy is 6.18 eV, in according with the above analysis.

Table 3 – Adsorption energies per H_2 for 1–4 H_2 molecules uptake on OBQ–Sc complex with and without vdW correction.

E_a(eV)/H_2	PBE	PBE-D2
H_2	0.07	0.12
$2H_2$	0.25	0.27
$3H_2$	0.21	0.25
$4H_2$	0.20	0.24

For C_6O_6 molecule, six C=O groups are adjacent to each other, suggesting that the complexes of C_6O_6-nSc are likely to form, where n denotes the number of Sc atoms. At Sc-rich condition, 3Sc atoms are inclined to bond with C_6O_6 in the most stable configuration where the carbon-ring has converted to benzene, as shown in Fig. 1e and Fig. S1 (supplemental material). The binding energy is 6.00 eV/Sc.

Hydrogen adsorption on OBQ–Sc complex

As discussed above, Sc/Ti atom tends to bond with two O atoms of OBQ. That is, the coordination number of TM in OBQ–Sc/Ti is two. As such, it provides enough empty *d* orbitals and space to accommodate H_2 molecules. Herein, we take OBQ–Sc complex as an example to discuss the potential of H_2 adsorption. The average adsorption energy (cf. Table 3) is defined as $E_a = (E_{OBQ-Sc} + nE_{H_2} - E_{OBQ-Sc-nH_2})/n$, where E_{OBQ-Sc}, E_{H_2}, and $E_{OBQ-Sc-nH_2}$ denote the total energies of OBQ–Sc complex, isolated H_2, and OBQ–Sc with adsorbed H_2, respectively, and n is the number of H_2 molecules. According to the symmetry of OBQ–Sc complex, we have tried many possible initial positions of H_2 molecules. Overall, four H_2 molecules can be compactly adsorbed on OBQ–Sc, with the adsorption energy of 0.20 eV/H_2 and the H_2 storage capacity of 5.0 wt%. The optimized configurations of four H_2 molecules adsorbed on OBQ–Sc complex successively are shown in Fig. 2a–2d, respectively.

The first H_2 has a rather weak interaction with OBQ–Sc complex with $E_a = 0.07$ eV. The H–H bond and the nearest Sc … H distance are 0.76 and 2.59 Å, respectively (c.f. Fig. 2a). From projected density of states (PDOS) (c.f. Fig. 2e), it is found that the σ orbital of H_2 is distributed in a narrow energy range far below Fermi level, corresponding to a higher localization. It is consistent with the fact that the H–H bond is nearly unchanged from the free state (0.75 Å), presenting a van der Waals (vdW) type of interaction.

However, for the adsorption of two H_2 molecules, they are inclined to locate at two sides of OBQ–Sc plane, showing a vertical symmetry. The bond lengths of two H_2 are both elongated to 0.82 Å. E_a is 0.25 eV/H_2 (0.43 eV for the second H_2), significantly larger than that of the first H_2. From the PDOS, the σ orbitals of H_2 are also located far below Fermi level, while there are hybridized states appearing in the energy range of [−1, 0] eV relative to Fermi level. The partial charge density (PCD), evaluated in this energy interval, shows an obvious node (depletion) between two H atoms. It indicates that the hybridization is attributed to the interaction between σ* orbitals of H_2 and *d* orbitals of Sc, consistent with the electron donation and back-donation process, showing a Kubas-like interaction character.

The third and fourth H_2 prefer to locate dispersedly at two sides of OBQ–Sc plane, with $E_a = 0.21$ and 0.20 eV, respectively. In particular, for the latter case, four H_2 molecules locate symmetrically around Sc atom with length of H_2 ~0.78 Å. In addition, we have conducted vdW corrections for the adsorption of 1–4 H_2 molecules on OBQ–Sc complex, as listed in Table 3. In comparison, vdW correction has the most significant effect on the first H_2 adsorption, 0.05 eV, nearly reaching to E_a obtained by

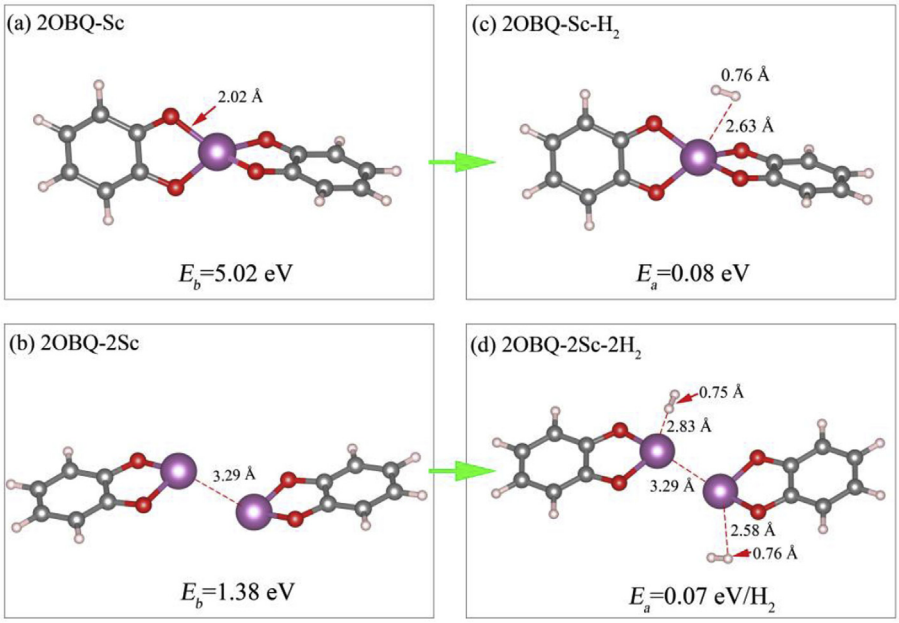

Fig. 3 – Optimized configurations for (a) an additional OBQ molecule adsorbing on OBQ–Sc complex (2OBQ–Sc), (b) two OBQ–Sc complexes clustering via Sc–Sc coupling (2OBQ–2Sc), (c) one H_2 molecule adsorption on 2OBQ–Sc, and (d) two H_2 molecules adsorption on 2OBQ–2Sc.

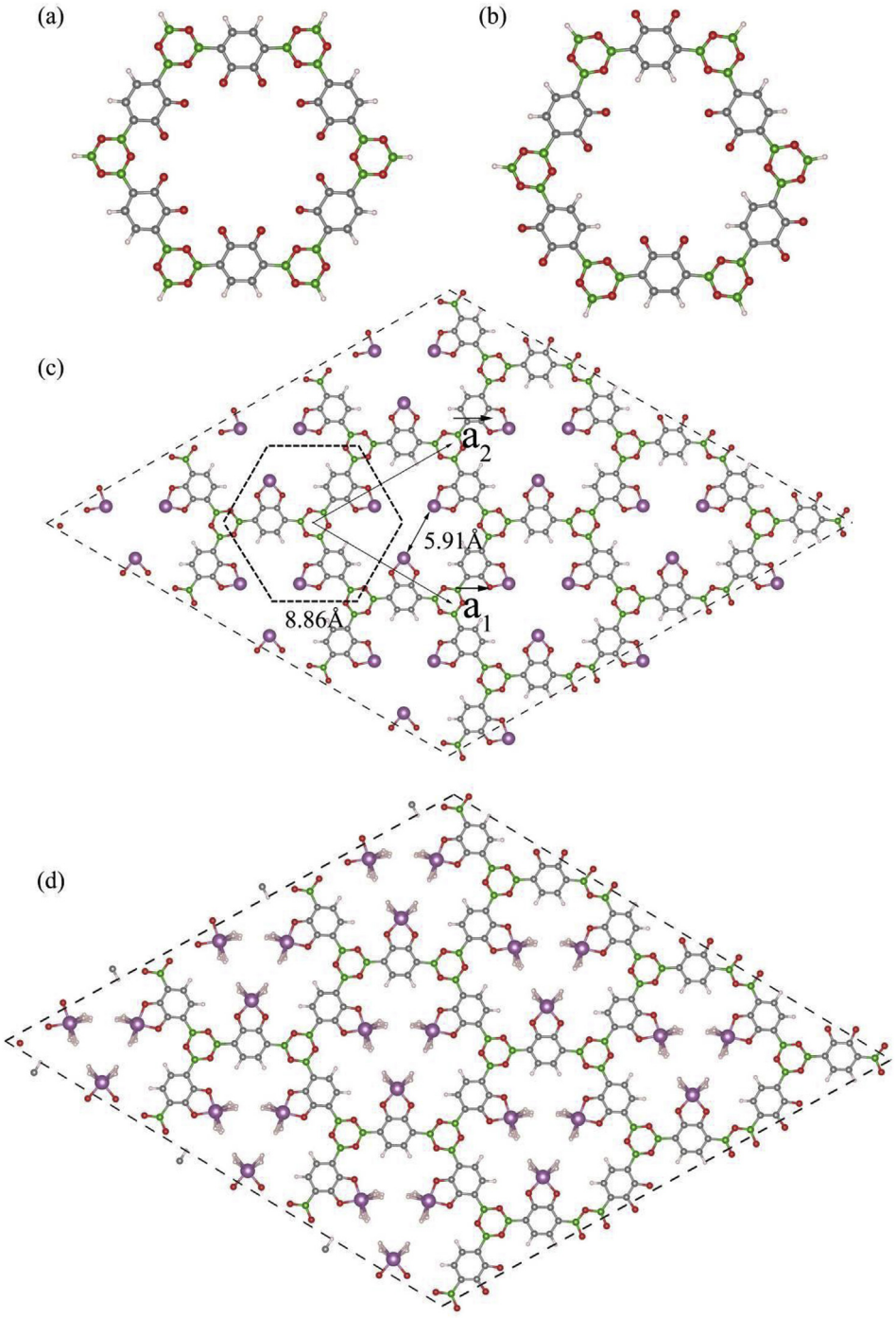

Fig. 4 – (a)/(b) The least/most stable configuration of $C_{36}O_{30}H_{18}B_{18}$ cluster. (c) Structure of modified COF-1 (MCOF-1). (d) H_2 uptake on MCOF-1. The gray, red, purple, white, and green balls denote C, O, Sc, H, and B atoms, respectively. (For interpretation of the references to color in this figure legend, the reader is referred to the web version of this article.)

PBE. This is because vdW interaction dominates the adsorption of the first H_2 on OBQ–Sc complex. However, for the second, third, and fourth H_2 adsorption, Kubas-like interaction becomes the domination with $E_a = 0.20–0.25$ eV/H_2. Compared to it, their vdW corrections, which are in the range of 0.02–0.04 eV/H_2, have a smaller contribution to the adsorption energy. Furthermore, we evaluate the applicable temperature for H_2 storage of OBQ–Sc complex. As shown in Fig. S2 (supplemental material), there is one platform for the release of H_2 at three different pressures. Under 1, 20, and 50 atmospheric pressures, each Sc atom can accommodate $4H_2$ at T < 180, 220, and 235 K, respectively, corresponding to H_2 storage capacity of 5 wt%.

Design of hydrogen storage media

As demonstrated above, OBQ shows great dispersing ability towards Sc atom with respect to Sc bulk structure. However, it should be stressed that in the formed OBQ–Sc complex, the Sc

atom still holds one valence electron, which is likely to lead to two possible scenarios: (i) The additional OBQ molecules further adsorb on Sc atom; (ii) The OBQ–Sc complexes form cluster via Sc–Sc coupling. The optimized configurations for these two cases are shown in Fig. 3a and 3b, with binding energies (E_b) of 5.02 and 1.38 eV, respectively. That is to say, the OBQ–Sc complexes are energetically favored to form higher coordinated organic-metal complex. Furthermore, we investigate the H_2 adsorption on these two configurations. It is found that no H_2 could be accommodated via Kubas-like interaction, seen in Fig. 3c and 3d. For example, the average adsorption energy (E_a) of H_2 on 2OBQ–Sc or 2OBQ–2Sc is ~0.07 eV, with the nearest distance between Sc and H atoms as large as ~2.6 Å, showing obvious vdW-type interaction. Thus, how to realize an isolated structure of OBQ–Sc is critical in material design for H_2 storage via Kubas-like interaction. On the other hand, a higher H_2 capacity is another key criterion for practical application. For OBQ–Sc complex, the storage capacity reaches up to 5.0 wt%, while it will decrease inevitably due to the introduction of other components. A practical approach is to choose some light elements such as C, H, B, etc., to construct an OBQ–Sc complex frame.

Covalent organic frameworks (COFs)

With the adsorption of Sc on OBQ, a remarkable change in structure is the transformation of the unsaturated carbon-ring to benzene. It is exactly the inverse process to the preparation of OBQ in experiments. Therefore, our structure design can be divided into two steps. (i) Search for the materials that are rich in benzene-rings; (ii) Transform the benzene into OBQ via certain chemical methods. In this respect, the covalent organic frameworks (COFs) are the potential candidates, where benzene-rings are the major components. Recently, it was reported that the COF pore walls can be functionalized with desired groups and preferred density via quantitative click reaction [41], which provides possibility for modifying the benzene-rings in COFs to OBQ molecules. In the following, we take one of the simplest COF materials, COF-1, as the representative model to discuss the possibility for H_2 storage.

In COF-1, four H atoms are located in pairs at two sides of benzene. As such, two types of orientations are possible for each OBQ in the modified COF-1 (MCOF-1). To confirm the most stable configuration, we adopt a cluster model with formula $C_{36}O_{30}H_{18}B_{18}$, and compare the total energies of all the possible configurations with different orientations of OBQ molecules. For comparison, the adjacent OBQ molecules are energetically favored to adopt an opposite orientation, as shown in Fig. 4b, which is about 1.73 eV more stable than the least stable one (c.f. Fig. 4a), where O atoms are all located within the ring. It is likely ascribed to the electrostatic repulsion between O atoms.

Note that MCOF-1 structure can be recognized as constituted by a series of this clusters, it is reasonable to speculate that OBQ molecules in MCOF-1 also tend to adopt this configuration. Compared to COF-1, which is chemically inert to bind enough H_2 at ambient conditions, MCOF-1 has become a reactive sorbent. Once Sc or Ti atoms are dispersed by OBQ molecules, the unsaturated carbon-rings will restore the structure of benzenes (c.f. Fig. 4c). More importantly, OBQ–Sc complex will keep isolated due to the constraint of B_3O_3 unit. In this way, the clustering of OBQ–Sc complex will not happen during H_2 uptake and release processes.

On the other hand, the adsorption of H_2 molecules proceeds at two sides of the MCOF-1 plane, and the distance between the nearest Sc atoms is as large as ~5.91 Å. This guarantees enough room for the H_2 uptake. Therefore, the

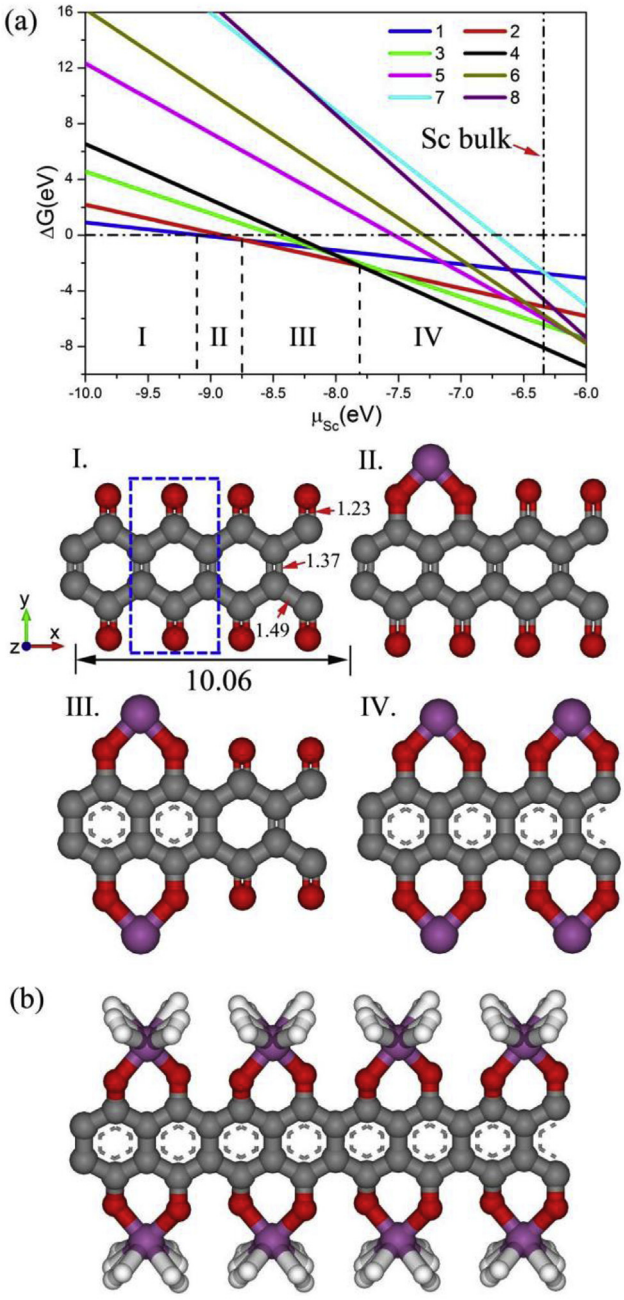

Fig. 5 – (a) Phase diagram of different number of Sc atoms (1–8) binding with periodic structure of $C_{16}O_8$. The structure in dashed box can be viewed as a PBQ. Insets I ($C_{16}O_8$), II ($C_{16}O_8$–Sc), III ($C_{16}O_8$–2Sc) and IV ($C_{16}O_8$–4Sc) correspond to the most stable configurations in energy regions of I, II, III, and IV that are marked in (a), respectively. (b) H_2 uptake on configuration III. Here it is doubled along the X direction for exhibition. The lengths are in Å.

adsorption of H_2 on MCOF-1 should be similar to that of isolated OBQ–Sc. The optimized configuration of H_2 uptake is shown in Fig. 4d. The capacity of H_2 storage reaches up to 3.8 wt%.

O-terminated zigzag graphene nanoribbons (O-ZGNRs)

As an isomer to OBQ, PBQ shows the same reaction mechanism when binding with TMs. Structurally, we note that the O-terminated zigzag graphene nanoribbons (O-ZGNRs) can be recognized as a polymer of PBQ molecule, which would be converted to benzene-rings after each O atom obtaining an electron. Here, we choose a periodic structure of $C_{16}O_8$ (c.f. Fig. 5a Inset I) to simulate the O-ZGNRs. The relative stability of $C_{16}O_8$ is evaluated from the formation energy in energy per atom of the structure with respect to its constitutes. Here graphene and the triplet state of O_2 are taken as the reference states. The formation energy (ΔH) of $C_{16}O_8$ is defined as $\Delta H = \frac{E(C_{16}O_8)}{24} - \frac{2}{3}\mu_C - \frac{1}{3}\mu_O$, where μ_C is the energy per atom of a single graphene sheet, and μ_O is the energy per atom of the triplet ground state of the O_2 molecule. The calculated ΔH is −0.21 eV, indicating that $C_{16}O_8$ is energetically stable, in good agreement with previous studies [38,42].

We investigate the adsorption of 1–8 Sc atoms on $C_{16}O_8$ and obtain their most stable configurations, respectively. To consider their relative stability, we calculate the Gibbs free energy via $\Delta G = E_T - E_P - n\mu_{Sc}$. Here, E_T and E_P denote the total energies of Sc-adsorbed $C_{16}O_8$ and pristine $C_{16}O_8$, and μ_{Sc} and n represent the chemical potential of Sc atom in the energy range of [−10, −6] eV and the number of Sc atoms.

According to the phase diagram, we find that 4 Sc atoms prefer to bond with 8 O atoms in two pairs along the two sides of $C_{16}O_8$, showing a central symmetry (c.f. Fig. 5a Inset IV), when the chemical potential of Sc is in the range of [−7.85, −6.34] eV. However, in the range of [−8.75,−7.85] eV, the configuration of 2 Sc atoms bonded with 4 O atoms in pair is favored (c.f. Fig. 5a Inset III). The binding energies for these two cases are 6.17 and 6.72 eV, respectively, both significantly larger than the cohesive energy of Sc. The H_2 storage property of $C_{16}O_8$–4Sc is similar to that of OBQ–Sc, i.e., each Sc atom accommodating four H_2 molecules, as shown in Fig. 5b. The adsorption energy is 0.21 eV/H_2, and the H_2 storage capacity reaches to 6.0 wt%.

Conclusion

In summary, we have theoretically investigated the adsorption of TM (TM = Sc, Ti, V, Cr, Mn, Fe, Co, Ni, Cu, and Zn) on OBQ. It is found that Sc/Ti atom is energetically dispersed by OBQ molecule with enough empty *d* orbitals for H_2 storage, since the coordination number of Sc/Ti in OBQ-Sc/Ti complex is only two. Four H_2 molecules can be accommodated by each OBQ–Sc complex via Kubas-like interaction mechanism, with adsorption energy of 0.20 eV/H_2 and storage capacity of 5.0wt %. Two structures have been proposed for H_2 storage using BQ molecule as building block. It is not only able to disperse Sc atoms, but also avoid the clustering of OBQ–Sc complexes, thereby being beneficial for the uptake and release of H_2.

Acknowledgments

This work was supported by NSFC (Grant No. 11474100, 51431001), Guangdong Natural Science Funds for Distinguished Young Scholars (Grant No. 2014A030306024), and the Fundamental Research Funds for the Central Universities (2015PT017, 2015ZP010). The computer times at National Supercomputing Center in Guangzhou (NSCCGZ) are gratefully acknowledged.

Appendix A. Supplementary data

Supplementary data related to this article can be found at http://dx.doi.org/10.1016/j.ijhydene.2016.05.033.

REFERENCES

[1] Kubas GJ. Metal–dihydrogen and σ-bond coordination: the consummate extension of the Dewar–Chatt–Duncanson model for metal–olefin π bonding. J Organomet Chem 2001;635:37–68.
[2] Yildirim T, Ciraci S. Titanium-decorated carbon nanotubes as a potential high-capacity hydrogen storage medium. Phys Rev Lett 2005;94. 175501.
[3] Zhao Y-f, Kim Y-H, Dillon AC, Heben MJ, Zhang SB. Hydrogen storage in novel organometallic buckyballs. Phys Rev Lett 2005;94. 155504.
[4] Chen M, Zhao Y-J, Liao J-H, Yang X-B. Transition-metal dispersion on carbon-doped boron nitride nanostructures: applications for high-capacity hydrogen storage. Phys Rev B 2012;86. 045459.
[5] Durgun E, Ciraci S, Yildirim T. Functionalization of carbon-based nanostructures with light transition-metal atoms for hydrogen storage. Phys Rev B 2008;77. 085405.
[6] Zou X, Zhou G, Duan W, Choi K, Ihm J. A chemical modification strategy for hydrogen storage in covalent organic frameworks. J Phys Chem C 2010;114:13402–7.
[7] Liu C, Fan YY, Liu M, Cong HT, Cheng HM, Dresselhaus MS. Hydrogen storage in single-walled carbon nanotubes at room temperature. Science 1999;286:1127–9.
[8] Pupysheva OV, Farajian AA, Yakobson BI. Fullerene nanocage capacity for hydrogen storage. Nano Lett 2008;8:767–74.
[9] Teprovich JA, Wellons MS, Lascola R, Hwang S-J, Ward PA, Compton RN, et al. Synthesis and characterization of a lithium-doped fullerane (Lix-C60-Hy) for reversible hydrogen storage. Nano Lett 2012;12:582–9.
[10] Yang SJ, Kim T, Im JH, Kim YS, Lee K, Jung H, et al. MOF-derived hierarchically porous carbon with exceptional porosity and hydrogen storage capacity. Chem Mater 2012;24:464–70.
[11] Serguei P, Tse JS, Yurchenko SN, Lyuben Z, Thomas H, Gotthard S. Graphene nanostructures as tunable storage media for molecular hydrogen. Proc Natl Acad Sci U. S. A 2005;102:10439–44.
[12] Li S, Jena P. Comment on "combinatorial search for optimal hydrogen-storage nanomaterials based on polymers". Phys Rev Lett 2006;97. 209601.
[13] Sun Q, Wang Q, Jena P, Kawazoe Y. Clustering of Ti on a C60 surface and its effect on hydrogen storage. J Am Chem Soc 2005;127:14582–3.

[14] Venkataramanan NS, Khazaei M, Sahara R, Mizuseki H, Kawazoe Y. First-principles study of hydrogen storage over Ni and Rh doped BN sheets. Chem Phys 2009;359:173–8.
[15] Lee H, Choi WI, Ihm J. Combinatorial search for optimal hydrogen-storage nanomaterials based on polymers. Phys Rev Lett 2006;97. 056104.
[16] Lee H, Choi WI, Nguyen MC, Cha M-H, Moon E, Ihm J. Ab initio study of dihydrogen binding in metal-decorated polyacetylene for hydrogen storage. Phys Rev B 2007;76. 195110.
[17] Lee H, Nguyen MC, Ihm J. Titanium-functional group complexes for high-capacity hydrogen storage materials. Solid State Commun 2008;146:431–4.
[18] Durgun E, Ciraci S, Zhou W, Yildirim T. Transition-metal-ethylene complexes as high-capacity hydrogen-storage media. Phys Rev Lett 2006;97. 226102.
[19] Dai J, Yuan J, Giannozzi P. Gas adsorption on graphene doped with B, N, Al, and S: a theoretical study. Appl Phys Lett 2009;95. 232105.
[20] Reunchan P, Jhi S-H. Metal-dispersed porous graphene for hydrogen storage. Appl Phys Lett 2011;98. 093103.
[21] Choi WI, Jhi S-H, Kim K, Kim Y-H. Divacancy-nitrogen-assisted transition metal dispersion and hydrogen adsorption in defective graphene: a first-principles study. Phys Rev B 2010;81. 085441.
[22] Lee H, Ihm J, Cohen ML, Louie SG. Calcium-decorated carbon nanotubes for high-capacity hydrogen storage: first-principles calculations. Phys Rev B 2009;80. 115412.
[23] Krasheninnikov AV, Lehtinen PO, Foster AS, Pyykkö P, Nieminen RM. Embedding transition-metal atoms in graphene: structure, bonding, and magnetism. Phys Rev Lett 2009;102. 126807.
[24] Choi WI, Wood BC, Schwegler E, Ogitsu T. Combinatorial search for high-activity hydrogen catalysts based on transition-metal-embedded graphitic carbons. Adv Energy Mater 2015;5. 1501423.
[25] Liao J-H, Zhao Y-J, Yang X-B. Controllable hydrogen adsorption and desorption by strain modulation on Ti decorated defective graphene. Int J Hydrogen Energ 2015;40:12063–71.
[26] Chandrakumar KRS, Srinivasu K, Ghosh SK. Nanoscale curvature-induced hydrogen adsorption in alkali metal doped carbon nanomaterials. J Phys Chem C 2008;112:15670–9.
[27] Gao F, Ding Z, Meng S. Three-dimensional metal-intercalated covalent organic frameworks for near-ambient energy storage. Sci Rep 2013;3.
[28] Kresse G, Furthmüller J. Efficient iterative schemes for ab initio total-energy calculations using a plane-wave basis set. Phys Rev B 1996;54:11169–86.
[29] Perdew JP, Ernzerhof M, Burke K. Rationale for mixing exact exchange with density functional approximations. J Chem Phys 1996;105:9982–5.
[30] Blöchl PE. Projector augmented-wave method. Phys Rev B 1994;50:17953–79.
[31] Grimme S. Semiempirical GGA-type density functional constructed with a long-range dispersion correction. J Comput Chem 2006;27:1787–99.
[32] Hu Z-X, Lan H, Ji W. Role of the dispersion force in modeling the interfacial properties of molecule-metal interfaces: adsorption of thiophene on copper surfaces. Sci Rep 2014;4:5036.
[33] Lü J-M, Rosokha SV, Neretin IS, Kochi JK. Quinones as electron acceptors. X-ray structures, spectral (EPR, UV–vis) characteristics and electron-transfer reactivities of their reduced anion radicals as separated vs contact ion pairs. J Am Chem Soc 2006;128:16708–19.
[34] van Bolhuis F, Kiers CT. Refinement of the crystal structure of p-benzoquinone at −160 °C. Acta Cryst 1978;34:1015–6.
[35] Albarran G, Boggess W, Rassolov V, Schuler RH. Absorption spectrum, mass spectrometric properties, and electronic structure of 1,2-Benzoquinone. J Phys Chem A 2010;114:7470–8.
[36] Kittel C. Introduction to solid state physics. Wiley; 2005.
[37] Knop O, Hartley JM. Refinement of the crystal structure of scandium oxide. Can J Chem 1968;46:1446–50.
[38] Ramasubramaniam A. Electronic structure of oxygen-terminated zigzag graphene nanoribbons: a hybrid density functional theory study. Phys Rev B 2010;81. 245413.
[39] Fattahi A, Kass SR, Liebman JF, Matos MAR, Miranda MS, Morais VMF. The enthalpies of formation of o-, m-, and p-benzoquinone: gas-phase ion energetics, combustion calorimetry, and quantum chemical computations combined. J Am Chem Soc 2005;127:6116–22.
[40] Altarawneh M, Dlugogorski BZ, Kennedy EM, Mackie JC. Theoretical study of unimolecular decomposition of catechol. J Phys Chem A 2010;114:1060–7.
[41] Nagai A, Guo Z, Feng X, Jin S, Chen X, Ding X, et al. Pore surface engineering in covalent organic frameworks. Nat Commun 2011;2:536.
[42] Hod O, Barone V, Peralta JE, Scuseria GE. Enhanced half-metallicity in edge-oxidized zigzag graphene nanoribbons. Nano Lett 2007;7:2295–9.